

Formation mechanism of toroidal rotation profile and characteristics of momentum transport in JT-60U

M. Yoshida, Y. Kamada, H. Takenaga, Y. Sakamoto, S. Ide, N. Oyama, H. Urano, T. Kobayashi, the JT-60 Team

Japan Atomic Energy Agency, Naka, Ibaraki-ken, 311-0193 Japan

e-mail contact of main author : yoshida.maiko@jaea.go.jp

Abstract. The diffusive term (the toroidal momentum diffusivity, χ_ϕ) and the non-diffusive term (the convection velocity, V_{conv}) of the momentum transport and the intrinsic rotation have been evaluated separately using the original transient momentum transport analysis. Thanks to the separation, characteristics of these terms are found for the first time as follows. (i) The characteristics of the momentum transport coefficients in the H-mode plasmas are obtained by plasma parameter scan such as plasma current (I_p), neutral beam (NB) heating power and electron density. The χ_ϕ increases with increasing the heat diffusivity (χ_i) over a wide range of radii and $\chi_\phi/\chi_i \sim 0.7-3$ at the middle of plasma $r/a=0.5$. (ii) The ratio of χ_ϕ/χ_i increases with increasing the ion temperature (T_i). (iii) the inward convection velocity ($-V_{conv}$) increases with increasing χ_ϕ , and $V_{conv}/\chi_\phi \sim -2.0 - -0.7$ (1/m) at $r/a=0.5$. (iv) We have also found that the intrinsic rotation with NBI, which is not explained with χ_ϕ , V_{conv} and the external momentum input, increases with increasing ion pressure gradient ($gradP_i$) and its direction is always antiparallel to I_p , i.e. the counter (CTR) direction. This dependence is almost the same, even the direction of the toroidal rotation velocity (V_t) and the confinement are different (I_p , L-mode, H-mode, CO-, BAL-, CTR-rotating plasmas). (v) We investigate the role of electron cyclotron heating on the V_t profile in the H-mode plasmas with low torque input using a fundamental O-mode electron cyclotron range of frequency wave (ECRF). It is supposed that the change in V_t with ECRF is due to the change in the momentum transport, the intrinsic rotation by $gradP_i$ and by ECRF itself. We separately estimate these terms, and found that ECRF drives the CO-intrinsic rotation inside the EC deposition and drives the CTR-intrinsic rotation outside the EC deposition. The CTR-rotation starts from the EC deposition location and the phase delay of the CTR-rotation is observed in the radial direction. This phase delay is comparable to χ_ϕ , which is obtained in the similar plasma condition.

1. Introduction

It is widely recognized that the toroidal rotation velocity (V_t) profiles play one of the most critical roles for plasma transport [1-3] and MHD stability [4-6]. However, the mechanism determining the V_t profile, which is determined by various terms (Fig. 1), has not been understood well. This is due mainly to an experimental difficulty in evaluating χ_ϕ , V_{conv} and the intrinsic rotation separately. In

order to address this issue, we have investigated the formation mechanism of V_t profile using the original transient experimental method in JT-60U [7-10].

In this paper, we investigate two topics, one is the momentum transport which influences the toroidal rotation profiles, and another is the intrinsic rotation by pressure gradient [9] and ECRF, respectively. In the last IAEA meeting [8], parameter dependences of χ_ϕ and V_{conv} in L-mode plasmas were reported using the transient experimental method. In this paper, after separating the diffusive and convective terms, the correlations between χ_ϕ , V_{conv} and χ_i in H-mode plasmas are discussed.

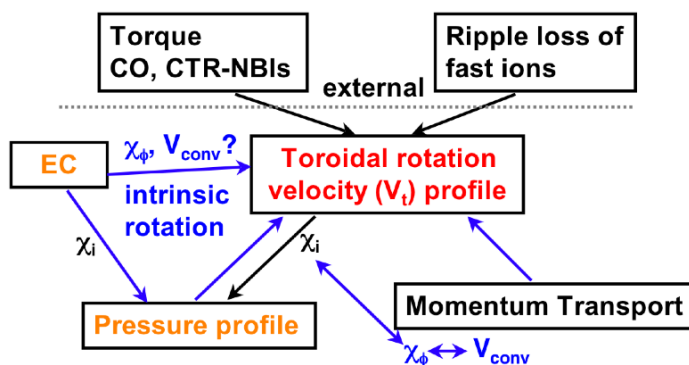


Fig. 1 Our approach for the investigation of the formation mechanism of the toroidal rotation velocity (V_t) profile.

Intrinsic toroidal plasma rotations generated by the plasma itself have recently become the subject of intense interest and investigation in the magnetically confined tokamak plasma research, since such an intrinsic rotation could dominate the total plasma rotation in future devices [11]. The worldwide progress in understanding the physics of momentum transport and rotation has been made experimentally [7-10, 12-19] and theoretically [20-24]. In this report, by separating the roles of external induced rotation and the intrinsic rotation on the measured V_t profiles using the original transient experiment method, we found the effect of plasma pressure on the intrinsic rotation in various confinement modes [9]. Concerning the toroidal rotation velocity with ECRF, it is supposed that the change in V_t is due to the change in (i) the momentum transport, (ii) the intrinsic rotation by the pressure gradient and (iii) the intrinsic rotation by ECRF itself. Because there was no experimental method to evaluate these factors separately, the formation mechanism of V_t profile with ECRF is not understood well. We define the V_t subtracted the change of V_t due to the momentum transport and $gradP_i$ from the measured V_t as an ECRF driven intrinsic, and have investigated the properties of the ECRF driven intrinsic rotation.

2. Experiment

Experiments were conducted in the JT-60U tokamak [25] where NBs of various injection geometries are installed. They consist of two tangential beams directing the same direction as that of the plasma current (CO-NBs), two tangential beams directing opposite to the plasma current (CTR-NBs) and seven near perpendicular (CO- and CTR-PERP) beams. For each of the CO and CTR direction, one of the tangential beams is almost on-axis deposition and the other is off-axis deposition, five of the PERP-NBs are almost on-axis deposition, and the others are off-axis. The injection angle of tangential beams is 36 degree and that of PERP-NBs is 75 degree with respect to the magnetic axis. The deuterium beam acceleration energy is about 85 keV, and the input power per injected unit is about 2 MW. Transient transport of toroidal momentum is demonstrated in the H-mode plasmas by using modulated injection of PERP-NBs, which enhances CTR rotation by the fast ion losses due to the toroidal field ripple in the peripheral region of the plasma [7]. The χ_ϕ and V_{conv} are evaluated from the toroidal momentum balance equation written as,

$$m_i \frac{\partial n_i V_t}{\partial t} = -\nabla \cdot \left\{ -m_i \chi_\phi \frac{\partial n_i V_t}{\partial r} + m_i V_{conv} n_i V_t \right\} + S, \quad (1)$$

where m_i , n_i , M and S are the ion mass, the ion density, the toroidal momentum flux and the toroidal momentum source, respectively [8]. In this report, ions are defined as the main (deuterium) and impurity ions, assuming that the toroidal rotation velocities of the main ions are the same as that of the carbon impurity ions, which is measured by the charge exchange recombination spectroscopy (CXRS) [26]. The negative sign of V_t and positive sign of one designate CTR- (in the opposite direction to I_p) and CO- (in the direction to I_p) directed rotation, respectively. Plasma parameters such as the plasma current (I_p), the neutral beam (NB) heating power (P_{ABS}), the electron density (n_e) and V_t are scanned in order to understand the characteristics of the momentum transport and the intrinsic rotation.

3. Characteristics of Momentum Transport Coefficients

In the last IAEA meeting [8], the characteristics of the momentum transport in L-mode plasmas are mainly discussed. In this section, the relations between χ_ϕ , χ_i and V_{conv} in H-mode plasmas are elucidated.

The momentum transport has a relation to the thermal ion heat transport as shown in Fig. 2. Figures 2(a)-2(c) shows the radial profiles of χ_ϕ , V_{conv} and χ_i , respectively, in an I_p scan for H-mode plasmas with low torque input. The toroidal magnetic field (B_T) also varies so that

the safety factor at 95% flux surface (q_{95}) is the same value of 3.9 ($I_p/B_T=1.2/2.6, 1.5/3.3, 1.8/3.8$ MA/T). For these plasmas, 2 units of CO tangential NB, 2 units of CTR tangential NB and 1-1.5 units of PERP-NBs are injected with $P_{ABS}=7.6-7.9$ MW. The line averaged electron density (\bar{n}_e) increases with increasing I_p as $\bar{n}_e=2.0-3.0 \times 10^{19} \text{ m}^{-3}$. The plasma volume ($Vol.$), the elongation at separatrix (κ_x) and the triangularity at separatrix (δ_x) are kept almost constant for this series of discharges ($Vol.=74 \text{ m}^3$, $\kappa_x=1.36-1.37$, $\delta_x=0.34-0.35$). The momentum diffusivity χ_ϕ decreases with increasing I_p over the whole radius. Such a dependence of χ_ϕ on I_p was observed in L-mode plasma [8]. Also χ_i decreases with increasing I_p . The comparison of χ_ϕ and χ_i for each I_p (1.2, 1.5 and 1.8 MA) in the region $0.2 < r/a < 0.6$ is shown in Fig. 2(d). These traces come from the profiles shown in Figs. 2(a) and 2(c), and the smaller values of χ_ϕ correspond to data in the inner region. One can see that χ_ϕ increases with increasing χ_i over a wide range of radii for each discharge.

The relations between χ_ϕ and χ_i in H-mode plasmas is elucidate at constant I_p of 1.2 MA. NB heating power and electron density scans are carried out under otherwise similar conditions ($B_T=2.5-2.6$ T, $\kappa_x=1.34-1.38$, $\delta_x=0.32-0.35$). The comparison of χ_ϕ and χ_i at $r/a=0.5$ is shown in Fig. 3(a). In this study, the relation between χ_ϕ and χ_i in the H-mode plasma is found after separating the diffusive and convective terms. We consider that the diffusivities χ_ϕ and χ_i at $r/a=0.5$ represent the quality of each global confinement and used towards the understanding of the relation (χ_ϕ and χ_i). Because a good correlation between χ_ϕ and χ_i was observed over a wide range of radii as shown in Fig. 2, and χ_i at $r/a=0.5$ has a good correlation with the thermal confinement time. The absorbed power varied over the range $5.6 \text{ MW} < P_{ABS} < 9.1 \text{ MW}$, and the electron density varies over the range $\bar{n}_e=2.0-3.0 \times 10^{19} \text{ m}^{-3}$ by varying gas puff rate. One can see that χ_ϕ increases with increasing χ_i , and the ratio of χ_ϕ/χ_i varies in the range of $\chi_\phi/\chi_i \sim 0.7-3$. Radial profiles of T_i and n_e for the plasmas of smaller $\chi_\phi/\chi_i \sim 1$ (denoted (A) and (c) in Fig. 3) and larger $\chi_\phi/\chi_i \sim 3$ (denoted (B) in Fig. 3) are described in Figs. 4(a) and 4(b). Concerning the difference of the operation regime between (A) and (B), P_{ABS} of (B) is larger than that of (A): $P_{ABS}=7.6 \text{ MW}$ for (B) and $P_{ABS}=5.6 \text{ MW}$ for (A). About (C), a large amount of D_2 gas of $10-30 \text{ Pa m}^3/\text{s}$ was puffed during NB injection with $P_{ABS}=6.1 \text{ MW}$. The T_i of larger χ_ϕ/χ_i case is larger

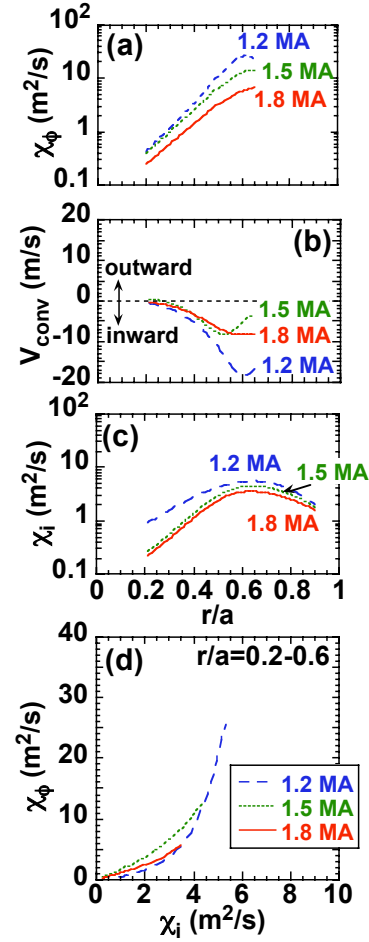


Fig. 2 Profiles of (a) the toroidal momentum diffusivity (χ_ϕ) and (b) the convection velocity (V_{conv}) obtained from beam perturbation techniques. (c) Profiles of the heat diffusivity (χ_i) in an I_p scan for H-mode plasmas at $q_{95}=3.9$, $P_{ABS}=7.6-7.9$ MW. (d) Comparison of χ_ϕ and χ_i for each I_p in the region $0.2 < r/a < 0.6$.

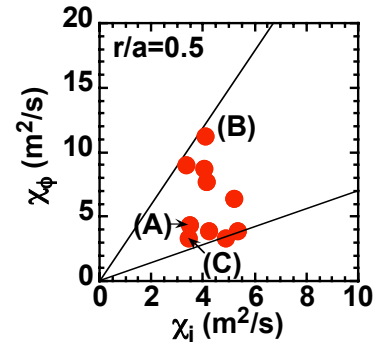


Fig. 3 (a) Relation of χ_ϕ and χ_i at $r/a=0.5$ during NB heating power and electron density scans in H-mode plasmas ($I_p=1.2 \text{ MA}$, $B_T=2.5-2.6$ T, $P_{ABS}=5.6-9.1 \text{ MW}$, $\bar{n}_e=2.0-3.0 \times 10^{19} \text{ m}^{-3}$).

than that of smaller $\chi_\phi/\chi_i \sim 1$ case. Such a dependence of χ_ϕ/χ_i on T_i has been found systematically as shown in Fig. 4(c). The ratio of χ_ϕ/χ_i at middle of plasma $r/a=0.5$ increases with increasing T_i . This is because that the growth of χ_i is larger than that of χ_ϕ as a function T_i . Although we examined parameter dependence of χ_ϕ/χ_i using other parameters such as n_e , the local ion pressure ($n_i T_i$), the normalized collisionality (ν^*), the normalized ion poloidal Larmor radius (ρ^*) at $r/a=0.5$, such a good dependence as shown in Fig. 4(c) could not be obtained. In this data set, the T_i gradient at $r/a=0.5$ is proportional to T_i at $r/a=0.5$. The result shown in Fig. 4(c) is consistent with that in L-mode plasmas shown in the last IAEA [8], where χ_ϕ/χ_i increases with increasing β_N , and then T_i linked with β_N .

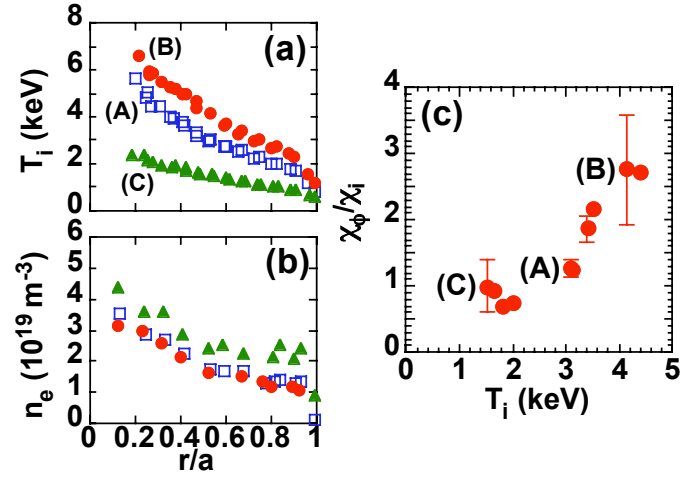


Fig. 4 Radial profiles of (a) the ion temperature (T_i) and (b) the electron density (n_e). Open squares (A) and triangles (C) indicate the plasma of smaller χ_ϕ/χ_i ($\chi_\phi/\chi_i \sim 1$), and solid circles (B) indicate the plasma of larger χ_ϕ/χ_i case ($\chi_\phi/\chi_i \sim 3$) shown in Fig. 3. (c) Dependence of χ_ϕ/χ_i on T_i at $r/a=0.5$.

The correlation between V_{conv} and χ_ϕ is also found using the same data set shown in Figs. 3 and 4. Figure 5(a) shows the correlation between $-V_{conv}$ and χ_ϕ in the region $0.25 < r/a < 0.6$ for each heating power and electron density. These traces come from the profiles of χ_ϕ and V_{conv} , and the smaller values of χ_ϕ correspond to those in the inner region. In the case with $\bar{n}_e = 2.7-3.0 \times 10^{19} \text{ m}^{-3}$, D_2 gas of $10-30 \text{ Pa m}^3/\text{s}$ was puffed during NB injection, in order to obtain the data of a high electron density regime. In the case with $\bar{n}_e = 1.9-2.2 \times 10^{19} \text{ m}^{-3}$, no D_2 gas was puffed during NB injection. The inward convection velocity ($-V_{conv}$) increases with increasing χ_ϕ over a wide range of radii for lower density ($\bar{n}_e = 1.9-2.2 \times 10^{19} \text{ m}^{-3}$). In the case with higher density ($\bar{n}_e = 2.7-3.0 \times 10^{19} \text{ m}^{-3}$), because $-V_{conv}$ decreases with plasma radius in spite of χ_ϕ increases, the decrease of $-V_{conv}$ with increasing χ_ϕ is observed. Also the correlation at fixed radius ($r/a=0.5$) is shown in Fig. 5(b). The inward convection velocity ($-V_{conv}$) increases with increasing χ_ϕ at the fixed radius $r/a=0.5$, and the value of $-V_{conv}/\chi_\phi$ is around 0.5 - 2 (1/m) in this data set. Parameter dependence of V_{conv}/χ_ϕ is area for future study, however, this finding of the correlation between χ_ϕ and V_{conv} can contribute to the understanding of the anomalous momentum transport [23].

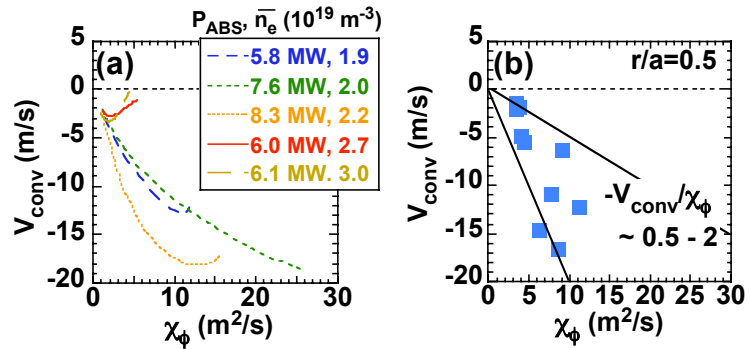


Fig. 5 Correlation between V_{conv} and χ_ϕ (a) from the profile data in the region $0.25 < r/a < 0.6$ for each discharge, and (b) at $r/a=0.5$ in H-mode plasmas. The same data set shown in Figs. 3 and 4 is used.

4. Intrinsic Rotation by Presser Gradient

The steady V_t profiles in the low β_N (<0.4) L-mode plasmas with and without external momentum input can be reproduced by the momentum transport equation using χ_ϕ and V_{conv} [7, 8]. The V_t profiles in higher β plasmas are investigated in this paper. Figure 6 illustrates the measured V_t profile (open circles) in an H-mode plasma ($\beta_N=1.29$, $I_p=1.2$ MA, $B_T=2.6$ T, $\delta_x=0.33$, $\kappa_x=1.43$). For these plasmas, 2 units of CO tangential NB and 2 units of PERP-NBs are injected with $P_{ABS}=6.0$ MW. The solid line in Fig. 6(a) shows the calculated V_t from the momentum transport equation using χ_ϕ and V_{conv} with the boundary condition (setting the measured V_t equal to the calculated one at $r/a\sim 0.65$) [7, 8]. The measured V_t deviates from the calculated one in the CTR-direction in the core region $0.25 < r/a < 0.45$, where a large ion pressure gradient ($gradP_i$) appears as shown in Fig. 6(b). In order to investigate the relation between the increase of CTR rotation and the $gradP_i$, the difference between the measured V_t and the calculated one (ΔV_t), i.e. the intrinsic rotation in the region $0.3 < r/a < 0.6$ is plotted against the $gradP_i$ in various plasmas in Fig. 6(c). In this data set, P_{ABS} and torque input are scanned. The symbols denote ΔV_t at $r/a=0.3, 0.4, 0.5$ and 0.6 . The larger values of $gradP_i$ are obtained in the core region. The data in a L-mode plasma at $\beta_N\sim 0.77$ is also plotted. As shown in Fig. 6(c), ΔV_t grows with increasing $gradP_i$ in all cases. This tendency is almost the same, even the direction of the V_t and the confinement are different (L-mode, H-mode, CO-, BAL-, CTR-rotating plasmas), over a wide range of χ_ϕ , which varies ~ 1 -30 m^2/s radially and ~ 1 -3 m^2/s (in the heating power scan) at fixed radius ($r/a\sim 0.4$). Moreover the dependence of ΔV_t on $gradP_i$ has been observed in different I_p as shown in Fig. 6(d), where the same data set shown in Fig. 2 is used ($q_{95}=3.9$, $I_p/B_T=1.2/2.6, 1.5/3.3, 1.8/3.8$ MA/T). Even in the different regime of I_p , the similar trace is shown. The good correlation between the local intrinsic rotation velocity and the local $gradP_i$ indicates that the $gradP_i$ causes the local CTR intrinsic rotation velocity [9].

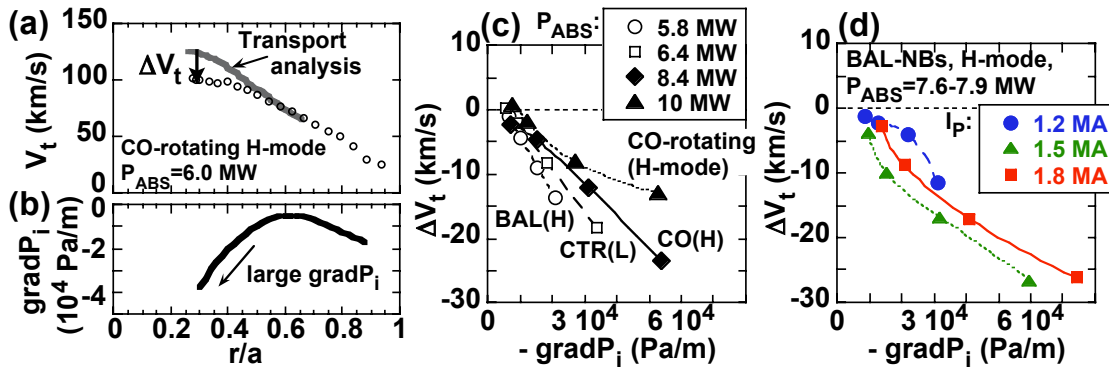


Fig. 6 (a) Profiles of the measured V_t (open circles) and the calculated one (solid line), (b) and $gradP_i$ in the case of the H-mode plasma ($I_p=1.2$ MA, $B_T=2.8$ T, $\beta_N=1.29$). (c) The difference between the measured V_t and the calculated one (ΔV_t) is plotted against the $gradP_i$ for each discharge (the CTR-rotating L-mode plasma at $I_p/B_T=1.5$ MA/3.8 T, CO- and BAL-rotating H-mode plasmas at fixed $I_p/B_T=1.2$ MA/2.6-2.8 T), and (d) in an I_p scan at fixed $P_{ABS}=7.6-7.9$ MW (the same data set in Fig. 2 is used). CTR intrinsic rotation (ΔV_t) increases with $gradP_i$ in all cases.

5. Role of ECRF on Toroidal Rotation

In this section, the effect of ECRF on V_t profile is discussed from the viewpoint of the intrinsic rotation by separating the effects of the change in the momentum transport and the change in the intrinsic rotation by $gradP_i$. We have found that ECRF increases the CTR-rotation outside the EC deposition and increases the CO-rotation inside the EC deposition in the H-mode plasma, and the CTR-rotation propagates from the EC deposition location to edge region. In this section, BAL-NBs injected plasmas are adopted in order to exclude the influence of the change in the momentum confinement as much as possible.

The response of V_t profile is investigated in a BAL-NBs injected plasma. The main plasma parameters for this plasma are $I_p=1.0$ MA, $B_T=3.8$ T, $\delta=0.33$, $\kappa=1.4$ and NB heating power is 7.6 MW. Figures 7(a) and 7(b) illustrate the waveforms of V_t at $r/a\sim 0.27$ and 0.38, respectively. Electron cyclotron wave of 2.7 MW is injected from $t=10$ s, and the EC deposition is at $r/a\sim 0.3$. The fundamental O-mode EC wave is used in this study. The V_t at $r/a\sim 0.27$ changes in the CO-direction, in other words, the CTR-rotation decreases. On the contrary, the V_t at $r/a\sim 0.38$ changes in the CTR-direction. The waveforms of T_i at $r/a\sim 0.27$, 0.38 and 0.43 are shown in Fig. 7(c). The T_i in core region decreases, then n_e is almost constant, therefore $gradP_i$ inside of $r/a\sim 0.3$ decreases with ECRF. Radial profiles of χ_i at $t=9.95$ s and 10.1 s are shown in Fig. 7(d). The thermal confinement degrades with ECRF.

Figure 8(a) shows the V_t profiles at $t=9.95$ s and 10.1 s in Fig. 7, and the difference in V_t between $t=9.95$ s and 10.1 s, i.e. the change in the measured V_t with ECRF, is plotted as solid circles and dotted line in Fig. 8(b). The measured V_t in the region $0.2 < r/a < 0.3$ changes in the CO-direction, on the other hand, the measured V_t in the region $0.3 < r/a < 0.6$ changes in the CTR-direction. The changes of V_t are caused by some factors. Firstly, the momentum transport coefficients (χ_ϕ and V_{conv}) affect the V_t profile [8], and these coefficients can vary with ECRF as χ_i shown in Fig. 7(d). Secondly, the intrinsic rotation driven by $gradP_i$ changes because $gradP_i$ degrades with ECRF. After subtracting these two factors from the changes in measured V_t with ECRF (solid circles and dotted line in Fig. 8), we can estimate the part of the intrinsic rotation driven by ECRF. In order to evaluate the intrinsic rotation driven by ECRF, we estimate the effects of the momentum transport and the intrinsic rotation by $gradP_i$ on V_t profile as follows.

The change in the momentum transport is estimated in a similar experimental condition ($I_p=1.0$ MA, $B_T=3.8$ T, NB heating power is 9.4 MW, EC power is 2.1 MW). It is found that the momentum transport degrades with ECRF as shown in Figs. 9(a) and (b). However the V_t

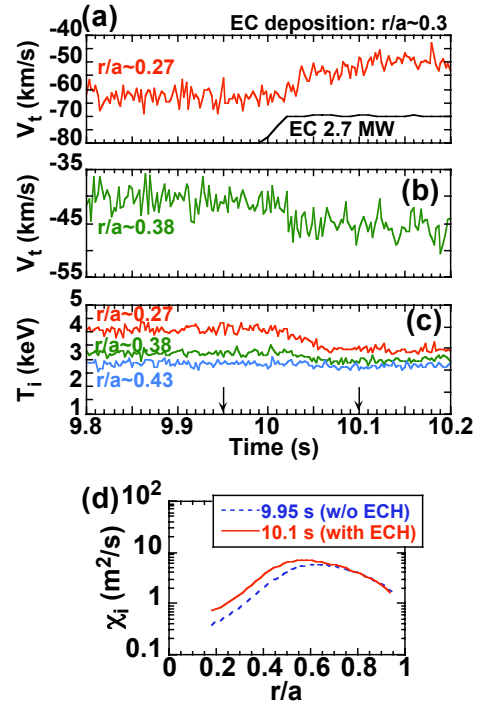


Fig. 7 Waveforms of (a) V_t at $r/a\sim 0.27$, (b) V_t at $r/a\sim 0.38$, and (c) T_i at $r/a\sim 0.27$, 0.38, 0.43. ECRF is injected at $t=10$ s, the input power is 2.7 MW and the deposition location is at $r/a\sim 0.3$. (d) Profile of χ_i at $t=9.95$ s and 10.1 s. ($I_p=1.0$ MA, $B_T=3.8$ T, $\delta=0.33$, $\kappa=1.4$ and NB power is 7.6 MW).

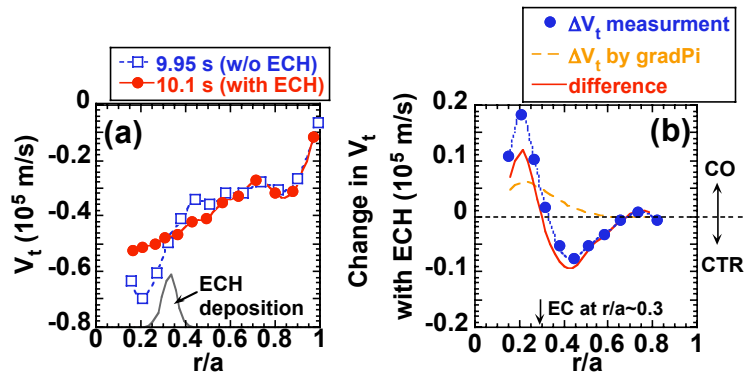


Fig. 8 (a) Profiles of the measured V_t at $t=9.95$ s and 10.1 s in Fig. 7. (b) Change in V_t with ECRF (solid circles and dotted line). Dashed line indicates the change in the intrinsic rotation by $gradP_i$ (predicted by the change in $gradP_i$, χ_ϕ and V_{conv} with ECRF). Solid line shows the difference in two lines, and means the intrinsic rotation by ECRF.

profile reproduced by χ_ϕ and V_{conv} hardly changes in the region $0.4 < r/a < 0.7$ because of the BAL-NB injection. The V_t at $r/a < 0.3$ tends to change in the CTR-direction, and the direction is opposite to the measurement as shown in Fig. 8. Because the absorbed power of CO-NBs is slightly larger than that of CTR-NBs, the torque input in core region is slightly positive (CO-direction). The flatness of the reproduced V_t at $r/a > 0.3$ comes from the degradation of momentum transport with the slight CO torque input in the core region.

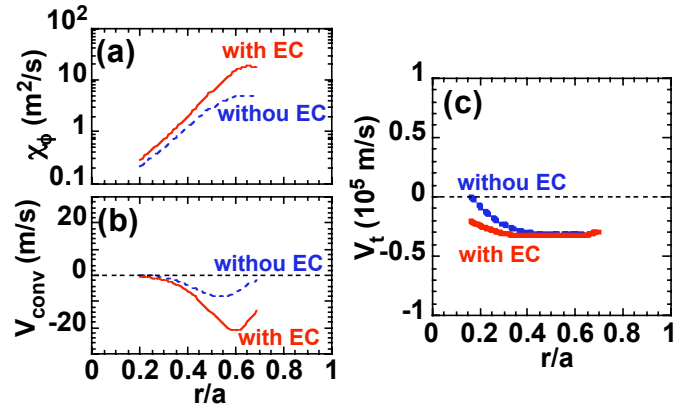


Fig. 9 Profiles of (a) χ_ϕ and (b) V_{conv} and (c) calculated V_t in the case with and without ECRF.

The change in the intrinsic rotation by $gradP_i$ is also estimated from the relation between the intrinsic rotation and $gradP_i$ (see section 4) in a similar experimental condition ($I_p=1.0$ MA, $B_T=3.8$ T, NB heating power is 9.4 MW, EC power is 2.1 MW). The dashed line in Fig. 8(b) shows the change in the intrinsic rotation by $gradP_i$. The degradation of $gradP_i$ increases the CO-rotation (reduce the CTR-rotation) and its region is mainly inside of $r/a \sim 0.4$. Thus, the increase of CTR-rotation in the region $0.4 < r/a < 0.6$ can not be explain by the change in $gradP_i$ and the momentum transport. The difference between the change in measured V_t with ECRF (dotted line) and the change in the intrinsic rotation by $gradP_i$ (dashed line) is plotted as solid line in Fig. 8(b). Even the effects of the momentum transport and $gradP_i$ are considered, we can conclude that ECRF yields the CTR-intrinsic rotation outside the EC deposition position ($r/a > 0.3$ in Fig. 8).

In order to clarify the region where the CTR-rotation increases with ECRF, the EC deposition scan is demonstrated. Figure 10(a) shows the change in measured V_t with ECRF for each EC deposition: $r/a \sim 0.3$, 0.45 and 0.6. The main plasma parameters for these plasmas are the same as that in Fig. 8 ($I_p=1.0$ MA, $B_T=3.8$ T, $R=3.4$ m, $a=0.9$ m, $\delta=0.33$, $\kappa=1.4$ and NB heating power is 7.5 MW). The EC power is 2.7 MW for $r/a \sim 0.3$ and 0.45 deposition, and 2.1 MW for $r/a \sim 0.6$ deposition. The region, where the CTR-rotation increases, varies with the EC deposition: the increase of the CTR-rotation is observed outside the EC deposition location and the increase of the CO-rotation is observed inside the EC deposition location. The time, when the CTR-rotation starts, is plotted against the plasma minor radius as open circles in Fig. 10(b). The time, when the CO-rotation starts, is also plotted as open squares. On can see, the CTR-rotation starts around the EC deposition location and propagates to the edge region. Such phase delay of the CO-rotation is not clear in this plasma. These results mean that ECRF itself increases the CTR-rotation outside the EC deposition location and increases the CO-rotation inside the EC deposition location. The propagation time is about 5 m/s in the region $0.4 < r/a < 0.6$ and is comparable to χ_ϕ at $r/a \sim 0.5$ shown in Fig. 9(a).

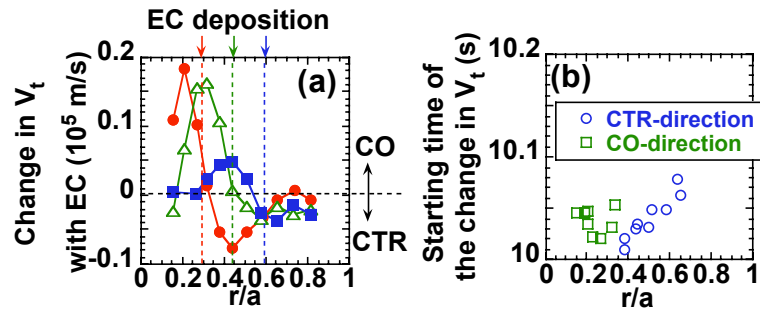


Fig. 10 Profiles of (a) χ_ϕ and (b) V_{conv} and (c) calculated V_t in the case with and without ECRF.

6. Summary

In this paper, the characteristics of the momentum transport coefficients (χ_ϕ , V_{conv}) evaluated from the transient analysis, the intrinsic rotation by pressure gradient and that by ECRF in H-mode plasmas are investigated. The toroidal momentum diffusivity (χ_ϕ) increases with increasing χ_i and $\chi_\phi/\chi_i \sim 0.7-3$ at $r/a=0.5$. The dependence of the ratio of χ_ϕ/χ_i on the ion temperature (T_i) is found: χ_ϕ/χ_i increases with increasing T_i . The correlation between V_{conv} and χ_ϕ is elucidated: the inward convection velocity ($-V_{conv}$) increases with increasing χ_ϕ , and $V_{conv}/\chi_\phi \sim -2 - -0.7$ (1/m) at $r/a=0.5$. By separating the roles of external induced rotation and the intrinsic rotation on the measured V_i profiles, the effect of plasma pressure on the intrinsic rotation in various confinement modes is found for the first time: the CTR-intrinsic rotation increases with increasing $gradP_i$. The mechanism of the change in V_i profile with ECRF has been clarified: ECRF changes the V_i profile due to the degradation of the momentum transport, the reduction of the intrinsic rotation by $gradP_i$ and the intrinsic rotation by ECRF itself. ECRF increases the CTR-intrinsic rotation outside the EC deposition location and increases the CO-rotation inside the EC deposition location. The CTR-rotation propagates from the EC deposition location to edge region with a time scale of ~ 5 m/s, which is comparable to χ_ϕ .

Acknowledgements

This work was partly supported by JSPS, Grant-in-Aid for Young Scientists (B) No 20740325. The authors acknowledge the members of the Japan Atomic Energy Agency who have contributed to the JT-60U projects.

References

- [1] SAKAMOTO, Y., et al., Nucl. Fusion **41** (2001) 865.
- [2] SYNAKOWSKI, E. J., et al., Nucl. Fusion **39**, (1993) 1733.
- [3] LUCE, T., et al., in Proceedings of the 21st IAEA Fusion Energy Conference, Chengdu, 2006 (IAEA, China, 2006) PD3
- [4] WARD, D. J., et al., Phys. Plasmas **2** (1995) 1570.
- [5] TAKECHI, M., et al., Phys. Rev. Lett. **98**, (2007) 055002.
- [6] REIMERDES, H., et al., Phys. Rev. Lett. **98**, (2007) 055001.
- [7] YOSHIDA, M., et al., Plasma Phys. Control. Fusion **48**, (2006) 1673.
- [8] YOSHIDA, M., et al., Nucl. Fusion **47**, (2007) 856.
- [9] YOSHIDA, M., et al., Phys. Rev. Lett. **100**, (2008) 105002.
- [10] YOSHIDA, M., et al., Plasma and Fusion Research, **3** (2008) S1007.
- [11] Special issue on Progress in the ITER Physics Basis [Nucl. Fusion **47**, S18 (2007)].
- [12] KIM, J., et al., Phys. Rev. Lett. **72**, (1994) 2199.
- [13] NAGASHIMA, K., et al., Nucl. Fusion **34** (1994) 449.
- [14] IIDA, K., et al., J. Phys. Soc. Jap. **67** (1998) 4089.
- [15] LEE, W. D., et al., Phys. Rev. Lett. **91**, (2003) 205003.
- [16] BORTOLON, A., et al., Phys. Rev. Lett. **97**, (2006) 235003.
- [17] De Vries, P. C., et al., Plasma Phys. Control. Fusion **48** (2006) 1693.
- [18] TALA, T., et al Nucl. Fusion **47**, (2007) 1012.
- [19] RICE, J. E., et al Nucl. Fusion **47**, (2007) 1618.
- [20] KIM, Y. B., DIAMOND, P. H., GROEBNER, R. J., Phys. Fluids **B3**, (1991) 2050.
- [21] B. COPPI, Nucl. Fusion **42**, (2002) 1.
- [22] GURCAN, O. D., DIAMOND, P. H., HAHM, T. S., et al., Phys. Plasmas **14**, (2007) 042306.
- [23] HAHM, T. S., DIAMOND, P. H., GURCAN, O. D. AND REWOLDT, G., Phys. Plasmas **14**, (2007) 072302.
- [24] PEETERS, A. G., ANGIONI, C. AND STRINTZI, D., Phys. Rev. Lett. **98**, (2007) 265003.
- [25] TAKENAGA, H. and the JT-60 TEAM, Nucl. Fusion **47**, (2007) S563.
- [26] YOSHIDA, M., et al., submitted to Fusion Eng. Des.